ON THE STATISTICAL CHARACTERISTICS OF LOG-COMPRESSED RAYLEIGH SIGNALS
Theoretical formulation and experimental results

Dmitry Kaplan, Qinglin Ma

Siemens Medical Systems, Inc.
Ultrasound Group
Issaquah, Washington

Abstract

This paper addresses the effects of nonlinear LOG compression on the amplitude of the backscattered signals. The changes in the statistical characteristics of signals were examined and correlated with the compression parameters. We develop an analytical formulation for the probability density function (PDF) of log-compressed amplitude signals. To obtain the theoretical PDF, a Rayleigh distributed signal is subjected to a scaled log-compression of the form $n_1 \ln(x)+n_2$. Such transformation is common in medical ultrasound image formation as it allows independent control over the dynamic range and gain of the displayed image. The resulting Fisher-Tippett PDF and its statistical parameters are derived and compared with the empirically measured statistics of ultrasound images of scattering phantoms. The comparisons reveal a great degree of similarity between theoretical PDF and the histogram of the image, even though the goodness-of-fit tests indicate statistical mismatch from theoretical model due to factors such as non-ideal log compression transfer, noise, envelope smoothing, etc..

Introduction

Over the years, statistical modeling of scattering phenomena has received considerable attention. In the field of medical ultrasound imaging, these techniques are used to predict the performance of scanners and to optimize the many programmable parameters that affect image quality. Image texture, or speckle, is an important area of investigation. Speckle is viewed either as noise (because it masks small difference in gray levels), or image signal (because it is associated with the microstructure of tissue parenchyma). Though speckle is not yet thoroughly understood, a number of investigations have contributed to our knowledge (Buckhardt, 1978; Abbott et al., 1979; 1982; Wagner et al. 1983).

It is argued that acoustic speckle arises due to coherent interference and can be treated similarly to laser speckle. Theoretical study of the first order statistical characteristics of speckle has resulted in methods for speckle reduction (Jellins et al., 1975; Buckhardt, 1978; Shattuck et al., 1981; Magnin et al., 1982), while the second-order statistics provides evidence of a relationship between speckle size and the imaging system characteristics (Flax et al., 1981, Smith and Wagner, 1984; Gregg et al., 1986; Wagner et al., 1988), and improves the models for texture generation in B-mode images (Dickson, 1982; Goodsitt et al., 1983; Foster et al., 1983; Oosterveld et al., 1985; Tuthill et al., 1988). These studies establish the foundations of acoustic speckle theory and raise the possibility of using the speckle information in medical diagnosis. However, these studies assume that the signal processing which takes place in an ultrasound scanner is linear. In practice, a nonlinear signal compression is commonly used to show weak signals on the same scale as the strong specular reflections. How this nonlinear compression changes the statistical characteristics and the nature of the relationship between the resulting statistical parameters and system characteristics are the major issues this paper addresses. Though Waag et al. (1991) examined the log-compression effects on the amplitude distribution of backscattered signals, they did not address the problem of the resulting probability density function of the compressed signal and its relationship to system and compression parameters.

In this paper we first briefly review the derivation of Rayleigh probability density function for the pre-compressed signal, then extend the theoretical derivation through the log-compression stage, and finally compare the pre-compressed and log-compressed theoretical results with experimental data. Although goodness-of-fit tests indicate statistical mismatch from the theoretical model, the theoretical probability density functions and the empirical histograms exhibit a great degree of similarity, and from the statistical parameters of log-compressed signal we can obtain information about imaging system.

Derivation of the PDF for the Log-compressed Rayleigh-distributed Data

We will start by reviewing the derivation of the Rayleigh distribution of scattering field amplitudes. A more complete version of this derivation can be found in Ishimaru (1978). Here we will simply present the summary. The scattering medium is modeled as a multitude of randomly distributed

1051-0117/93/0000-0961 $4.00 © 1993 IEEE

scatterers. It is further assumed that the resolution cell of the ultrasound scanner contains a large number of these scatterers. (A resolution cell's size is defined by the equivalent width of an acoustic beam and the receiver time gating) .

Our task is to derive the probability distribution of the amplitude Z and phase φ of a scattered field. If we represent the scattered field E_s as a sum of "quadrature components" I and Q, we have

$$E_s = Z\exp(i\varphi) = I + iQ \qquad (1)$$

with $I = Z\cos(\varphi)$ and $Q = Z\sin(\varphi)$. As both quadrature components consist of contributions from many different particles, we deduce under the central limit theorem that both I and Q are normally distributed. As the phase φ is uniformly distributed over 2π (lacking the presence of any coherent fields) and independent of the amplitude Z, it can be shown that the probability distribution of the amplitude

$$Z = \sqrt{I^2 + Q^2},$$

is given by

$$f_z(z) = \frac{d}{dz}F_z(z) = \frac{z}{\sigma^2}\exp\left(\frac{-z^2}{2\sigma^2}\right)\mathrm{U}(z) \qquad (2)$$

Where

$$\mathrm{U}(z) = \begin{cases} 1 \text{ if } z \geq 0 \\ 0 \text{ if } z < 0 \end{cases}$$

and

$$\sigma^2 = \langle I^2 \rangle = \langle Q^2 \rangle.$$

A typical commercially available ultrasound scanner does not display the true magnitude z of the returned echo due to its large dynamic range. Instead, one of several compression techniques is applied to the envelope detected data before it is scan-converted and displayed on a monitor. A common compression technique is computing the logarithm of z. Let us investigate how this process affects the statistics of the scattered field.

We subject z to a scaled and shifted log compression to form a new random variable $\mathbf{Y}$:

$$\mathbf{Y} = n_1 \ln(\mathbf{Z}) + n_2 \qquad (3)$$

For some constant n_1 and n_2. (Note that n_1 is associated with the dynamic range of the particular scanner and n_2 with the gain setting). Also note that we are conveniently ignoring what happens when Z is 0.
The density function of $\mathbf{Y}$ is then given by

$$f_Y(y) = \frac{f_Z(z)}{\left|\frac{dy}{dz}\right|} \qquad (4)$$

Which, having noted that

$$z = \exp\left(\frac{y - n_2}{n_1}\right)$$

and

$$\frac{dy}{dz} = \frac{n_1}{z} = \frac{n_1}{\exp\left(\frac{y - n_2}{n_1}\right)}$$

simplifies to

$$f_Y(y) = \frac{1}{\beta}\exp(-g - \exp(-g)) \qquad (5)$$

Where

$$g = \frac{\alpha - y}{\beta},$$

$$\alpha = \frac{n_1 \ln(2\sigma^2)}{2} + n_2$$

$$\beta = \frac{n_1}{2}$$

The probability density function $f_Y(y)$ is of the Fisher-Tippett (or doubly exponential) form. Notice that the distribution's variable g is itself a function of the Rayleigh distribution's σ as well as the control parameters n_1 and n_2 of the compression. Armed with this knowledge, we can theoretically predict the mean and variance of the compressed data

$$\mathrm{E}(y) = \alpha - \gamma\beta = \frac{n_1 \ln(2)}{2} + n_1 \ln(\sigma) - \frac{\gamma n_1}{2} + n_2 \qquad (6)$$

$$\mathrm{E}\left((y - \bar{y})^2\right) = \frac{(\pi\beta)^2}{6} = \frac{\pi^2 n_1^2}{24} \qquad (7)$$

Where $\gamma \approx 0.5772$ is the Euler constant.
Conversely, we can determine the compression parameters n_1 and n_2 from the mean and variance of the log-compressed data. Given experimentally measured mean M and variance V of the log-compressed amplitude of the acoustic echo arising from a collection of Rayleigh scatterers, we arrive at

$$n_1 = \frac{2\sqrt{6}}{\pi}\sqrt{V} \qquad (8)$$

$$n_2 = \frac{1}{\pi}\left(-\sqrt{6V}\ln(2\sigma^2) + \pi M + \gamma\sqrt{6V}\right) \qquad (9)$$

Which results in the following empirical estimation of the parameters of the doubly-exponential distribution:

$$\alpha = M + \frac{\gamma\sqrt{6V}}{\pi} \qquad (10)$$

$$\beta = \frac{\sqrt{6V}}{\pi} \qquad (11)$$

It is important to note the physical meaning of n_1 and n_2. Indeed, n_1 is closely associated with the dynamic range of the ultrasound scanner being used and is independent of the target

and gain settings. n_2 is proportional to the overall system gain and is a function of system TGC setting. The importance of the two equations above lies in the opportunity to determine the dynamic range of the scanner from the variance of pre-scan-converted data and to determine the overall gain from the variance and mean of the log-compressed amplitude and the Rayleigh coefficient σ of the pre-compressed amplitude. We shall see below how this is accomplished.

Experimental Results

To experimentally confirm our theoretical results, we used a Siemens Quantum Q2000 ultrasound scanner to collect pre- and post-log-compressed scattering data. A block diagram of the pertinent signal path is shown below:

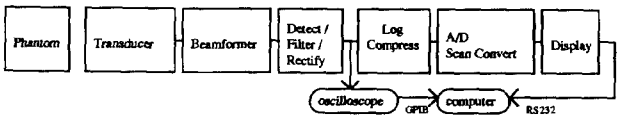

Figure 1. Block diagram of the experimental setup.

The following system configuration was selected:

System: Tissue only mode (i.e. no 2D Doppler information was collected)
One transmitter focal zone per acoustic beam mode selected.
60db dynamic range, log compressed.
Pre-processing and post-processing functions disabled, scan converter in a by-pass mode (NB it is critical that the data are collected with the scan converter disabled. The very process of interpolative scan conversion will, at the very least, reduce the variance of data).
Single cycle (at the transducer center frequency) transmit.

Transducer: 5L45 linear probe (5 MHz center frequency).

Phantom: Two types of acoustic phantoms were used. One was a commercially produced RMI tissue equivalent phantom, the other was a "slurry" phantom consisting of graphite particles suspended in a mixture of water and ethylene glycol. As the RMI phantom contains various targets designed to evaluate the performance of ultrasound scanners but which would have detrimental effect on our experiment, we have selected a region lacking any such features. We have also found it useful to submerge the RMI phantom in a water bath to improve acoustic coupling. (NB the slurry phantom was homogeneous.). The following were verified:
RMI phantom: attenuation: 0.5 dB/cm MHz,
Speed of sound: 1540 m/sec.
Slurry phantom: attenuation: 0.25 dB/cm MHz Speed of sound: 1508 m/sec.

Oscilloscope: Tektronix 2430A synchronized to the pulse repetition frequency (PRF).
5 MHz digitization rate.

Computer: A 386-class Personal Computer.

The envelope-detected pre-compressed A-line signal was digitized with the oscilloscope and recorded on a PC. The data from 41 acoustic beams of 98 samples each taken from a depth region of about 3 to 6 cm were collected. The corresponding compressed signal was collected on the computer via an RS232 interface to the scan converter.

Results

According to (2), the pre-compressed signal captured with the oscilloscope should have Rayleigh probability density function (PDF). To verify that we should determine the corresponding σ and perform a chi-square analysis of the fit. To find σ we have a choice of computing it from the various central moments of the captured data. We have selected to compute σ from the variance (i.e. second central moment) of the data for the following reasons:
1) even though the oscilloscope was DC coupled, it is still possible that an unaccounted-for DC shift will affect the mean of the data.
2) moments higher than the second require more and more data to be reliable and are more subject to outliers and noise (see Appendix B for some discussion of this).

Computed as stated, the σ_{slurry} was 30.18 and σ_{RMI} was 7.13. (The large difference between the σ's is probably related to the difference in the scatterer size distribution in the phantoms.) With σ's computed, measured data were DC-shifted to superimpose their mean onto the theoretical mean for the Rayleigh distribution (see Appendix A). This procedure compensated for the aforementioned DC-shift of the measurement. Histograms of the measured values were then calculated and somewhat smoothed to compensate for the oscilloscope's tenacious propensity for generating preferred codes.
Figure 2 shows the measured and theoretically predicted (Rayleigh) PDF for both phantoms. While the χ^2 test revealed that the measured data are not Rayleigh distributed, the similarities between the measured and theoretically predicted curves indicate that we are on the right track (χ^2 values were 65.5 with 19 degrees of freedom and 53.4 with 83 degrees of freedom for RMI and slurry phantoms respectively). The large values of χ^2 are probably due to a number of difficult to model events: frequency dependent attenuation, finite beam width and overlap, non-ideal log transformation, clipping of gray-scale data at the log amplifier, etc.

The post-compressed data were analyzed in a similar fashion: their mean and variance were computed and (6)-(11) were used to compute the following table:

Phantom	n_1	n_2	α	β	SNR	Dynamic Range
RMI	14.9	7.33	41.82	7.46	1.96	69.8 dB
slurry	13.7	15.9	67.15	6.83	2.34	76.3 dB

Table I. Computed parameters for the log-compressed amplitude data (SNR is computed as a ratio of the mean to standard deviation)

In the above table, dynamic range (DR) was computed as

$$\mathrm{DR} = 20\log\frac{A}{a};$$

(Here: A is the strongest allowable signal and
a is the weakest).

with

$(n_1 \ln A + n_2) - (n_1 \ln a + n_2) = (\text{total number of grey levels})$, we have:

$$\frac{\mathrm{DR}}{\text{total number of grey levels}} = \frac{20}{n_1 \ln(10)} \qquad (12)$$

Notice the relatively high degree of agreement for the value of n_1 for the two types of phantoms, indicating, as we mentioned before, that this parameter depends on the scanner and not the target. Notice further that the value of n_2 is approximately double for slurry phantom compared to that of an RMI phantom. This is explained by us having to apply half the TGC for the slurry phantom (due to the difference in attenuation coefficients).

Figure 3 shows the comparison between the measured and the predicted distributions of grayscale. Note the high degree of agreement (although the χ^2 again indicate that the measured distribution is not truly double exponential).

Conclusion

In this paper we have developed an analytical formulation for the PDF of a log-compressed amplitude of an echo from a collection of Rayleigh scatterers. We have demonstrated how the insight lets us determine the effective dynamic range of ultrasound scanners, and, with some instrumentation, the overall gain.

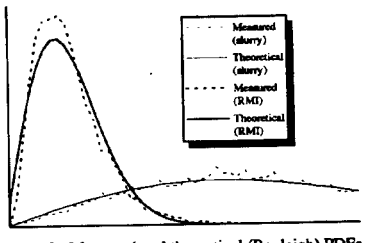

Figure 2. Measured and theoretical (Rayleigh) PDFs for RMI and slurry pre-compressed echo amplitude data.

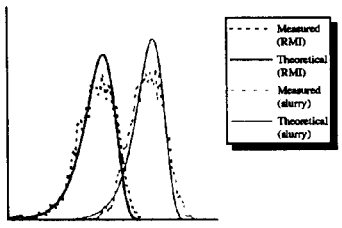

Figure 3. Measured and theoretical (double exponential) PDFs for RMI and slurry log-compressed echo amplitude data. (See Table I for the values of control parameters)

Bibliography

Abbott, J. G., and Thurstone, F. L. (1979). "Acoustic speckle: Theory and experimental analysis," Ultrasound. Imag., vol. 1, 303-324.

Burckhardt, C. B. (1978). "Speckle in ultrasound B-mode scans," IEEE trans. Sonics Ultrason., vol. 25, p. 1-6.

Dickson, R. J. (1982). "A computer model for speckle in ultrasound images: theory and application," Acoustical Imaging, vol. 10, A. F. Metherell, Ed., New York: Plenum, 115-129.

Flax, S. W., Glover, G. H., and Pelc, N. J. (1981). "Textural variations in B-mode ultrasonography: A stochastic model," Ultrason. Imag., vol. 3, No. 3, 235-257.

Foster, D. R., Arditi, M., Foster, F. S., Patterson, M. S., and Hunt, J. W. (1983). "Computer simulations of speckle in B-scan images," Ultrason. Imag., vol. 5, no. 4, 308-330.

Goodsitt, M. M., Madsen, E. L., and Zagzebski, J. A. (1983). "A three-dimensional model for generating the texture in B-scan ultrasound images," Ultrason. Imag., vol. 5, no. 3, 253-279.

Ishimaru, A. (1978). *Wave Propagation and Scattering in Random Media, Vol. I*, 89 - 92 (Academic Press, New York).

Jellins, J., Kossoff, G., Reeve, T. S., Barraclough, B. H. (1975). " Ultrasonic gray scale visualization of breast disease," Ultrasound in Med. & biol., vol. I, 393-404.

Magnin, P. A., Ramm, O. T. von, and Thurstone, F. L. (1982). "Frequency compounding for speckle contrast reduction in phased array images," Ultrasonic Imaging, vol. 4, 267-281.

Oosterveld, B. J., Thijssen, J. M., and Verhoef, W. A. (1985). "Texture B-mode images: 3-D simulations and experiments of the effects of diffraction and scatterer density," Ultrason. Imag., vol. 7, no. 2, 142-160.

Shattuck, D. P. and Ramm, O. T. von (1981), "Compounding scanning with a phased array," Ultrasound Imaging, vol. 4, 93-107.

Trahey, G. E., Smith, S. W., and Von Ramm, O. T. (1986). "Speckle pattern correlation with lateral aperture translation: experimental results and implications for spatial compounding," IEEE Trans. Ultrason., Ferroelect. Freq. Contr., vol. 33, No. 3,. 257-264.

Tuthill, T. A., Sperry, R. H., and Parker, K. J. (1988). "Derivations from Rayleigh statistics in ultrasonic speckle," Ultrason. Imag., vol. 10, no. 2, 81-89.

Waag, R., Demczar, B. and Case, T. J. (1991). "Nonlinear receiver compression effects on the amplitude distribution of backscattered ultrasonic signals," IEEE Trans. Biomedical Engineering, vol. 38, no. 7, 628-633.

Wagner, R. F., Smith, S. W., Sandrik, J. M., and Lopez, H. (1983). "Statistics of speckle in ultrasound B-scans," IEEE trans. Sonics Ultrason., vol. 30, 156-163.

Wagner, R. F., Insana, M. F., and Smith, S. W. (1988). "Fundamental correlation lengths of coherent speckle in medical ultrasonic images," IEEE Trans. Ultrason. Ferroelect. Freq. Contr., vol. 35, 34-44.

Abramowitz, M. A. and Stegun, I. A, ed, (1972). *Handbook of Mathematical Functions*, 8th printing, (Dover Publications, New York)